Experiments in Fluids (2018) 59:176
https://doi.org/10.1007/s00348-018-2635-8

RESEARCH ARTICLE

CFD and MRI studies of hemodynamic changes after flow diverter implantation in a patient-specific model of the cerebral artery

S. V. Frolov[1] · S. V. Sindeev[1] · J. S. Kirschke[2] · P. Arnold[2] · S. Prothmann[2] · D. Liepsch[3] · A. Balasso[4] · A. Potlov[1] · I. Larrabide[5] · S. Kaczmarz[2]

Received: 24 May 2018 / Revised: 11 October 2018 / Accepted: 13 October 2018

Abstract

Flow changes after flow diverter (FD) placement may be assessed by 4D phase-contrast MR-angiography (4D flow MRI) or simulated by computational fluid dynamics (CFD). However, cross-validation and future assessments with both approaches to take advantage of their individual strengths are required. In this study, we investigate the influence of a FD on intra-aneurysmal blood flow using both MRI experiments and CFD simulations. MR measurements were performed in a true-to-scale silicone model of a wide-neck saccular aneurysm of the distal internal carotid artery before and after FD deployment. An experimental setup, including a computer-controlled piston pump, was assembled to simulate pulsatile blood flow. For CFD studies, a virtual stenting technique was used to place a FD into the aneurysm model. Boundary conditions were applied according to MRI-measured flow data. A qualitative and quantitative agreement of velocity fields measured by CFD and MRI both before and after FD placement was demonstrated. The intra-aneurysmal flow reduction in the CFD results was 19%, while a reduction of 23% was measured by 4D flow MRI. Despite of the low spatial resolution, MRI was able to correctly determine the flow pattern in the aneurysm. The pre-treatment CFD simulation could be helpful in predicting the outcome of a FD treatment, while a post-interventional MRI could prove the desired treatment effect.

Graphical abstract

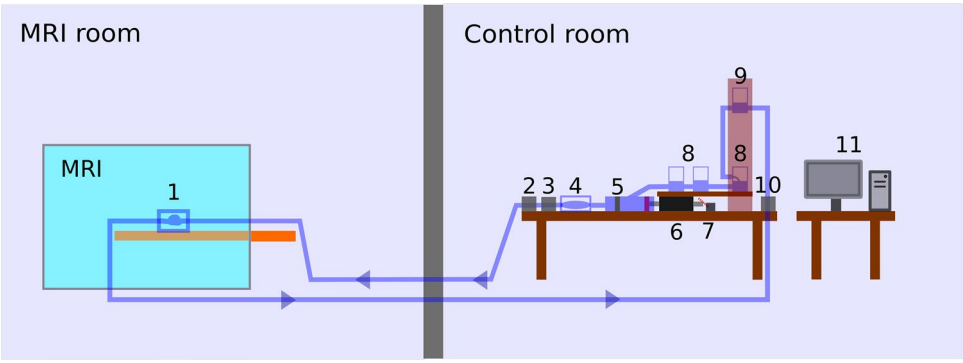

✉ S. V. Sindeev
ssindeev@yandex.ru

[1] Department of Biomedical Engineering, Tambov State Technical University, 106, Sovetskaya Street, Tambov 392000, Russian Federation

[2] Department of Diagnostic and Interventional Neuroradiology, Klinikum rechts der Isar, Technical University of Munich, Munich, Germany

[3] Department of Building Services Engineering and Print and Media Technology, Munich University of Applied Sciences, Munich, Germany

[4] Department of Earth and Environmental Sciences, Ludwig Maximilian University of Munich, Munich, Germany

[5] Pladema–CONICET, UNICEN, Tandil, Argentina

Published online: 01 November 2018

1 Introduction

A flow diverter (FD) is a modern device for treatment of un-coilable, wide-neck side-wall aneurysms and dysplastic parent vessels. The first FDs were used in clinical practice since 2007 and showed a high occlusion rate (Wong et al. 2011; Pierot and Wakhloo 2013; Walcott et al. 2016). The goal of a FD is to adjust the flow to its natural path using a braided fine mesh stent. However, the hemodynamic alterations caused by FD implantation cannot be precisely predicted (Zanaty et al. 2014). In some cases a FD even increased an inflow jet to the aneurysm sac which led to growth and rupture of the aneurysm (Darsaut et al. 2013). Thus, several studies reported ruptures of aneurysms after FD placement (Cebral et al. 2011; Kulcsár et al. 2011; Turowski et al. 2011; Chitale et al. 2014; Rouchaud et al. 2016). To prevent such scenarios, simulations before FD placement as well as a non-invasive quantification of the blood flow after FD placement is highly wanted to guide clinical decisions.

A number of studies were done to evaluate hemodynamic changes after treatment with a FD. Larrabide et al. demonstrated that the hemodynamics after FD placement strongly depends on aneurysm morphology as well as position and orientation of the aneurysm with respect to parent artery (Larrabide et al. 2015). Mut et al. found that the occlusion time of cerebral aneurysms treated with FDs can be predicted by the hemodynamic conditions created immediately after stent implantation (Mut et al. 2015). Specifically, low postoperative flow velocity, inflow rate, and shear rate are associated with fast occlusion. Ouared et al. suggested the criterion, which states that for successful treatment with a FD, the postoperative velocity in the aneurysm should be reduced by at least one-third compared to the preoperative condition (Ouared et al. 2016). The considered studies were done using Computational Fluid Dynamics (CFD).

However, of particular interest for physicians are methods which allow evaluating the intra-aneurysmal flow in vivo. One of such methods is magnetic resonance imaging (MRI), which is a promising non-invasive method for analyzing intracranial hemodynamics (Papaharilaou et al. 2001; Isoda et al. 2006; Naito et al. 2012; Muir et al. 2014; Berg et al. 2014; Karmonik et al. 2014; Kono and Terada 2014). Several groups have used MRI velocity measurements to estimate directly the hemodynamic characteristics in the aneurysm region. Papathanasopoulou et al. (2003) found a good general agreement between MRI-derived and CFD-predicted results for a physiologically realistic model of the human carotid bifurcation. van Ooij et al. (2013) observed that for low velocities the flow patterns for MRI and CFD were different due to the low signal-to-noise ratio (SNR) of MRI measurements. In Boussel et al. (2009), it was shown that direct MRI measurements of velocity magnitude, maximum shear stress and wall shear stress (WSS) distribution had a good agreement in comparison with patient-specific CFD prediction. Nevertheless, the absolute values of WSS were different between two techniques. This reflects the fact that CFD is capable of much higher resolution than MRI.

Recent studies showed the feasibility of using MRI for assessment of intra-aneurysmal flow alteration after FD placement (MacDonald et al. 2015; Pereira et al. 2015). In a feasibility study (Pereira et al. 2015), it was concluded that MRI in the context of FD could be of great value for validating or cross-validating CFD studies. Both approaches have advantages: CFD could be used to simulate outcomes before FDs are placed and has much higher spatial and temporal resolution, but requires many assumptions that might be met or not, while 4D flow MRI presents quantitative measures obtained without models or assumptions, but with measurement errors and limited spatial and temporal resolution. Therefore, cross-validation and future assessments with both approaches to take advantage of their individual strength are required.

The aim of the present study is to investigate the influence of a FD on intra-aneurysmal blood flow using both MRI experiments and CFD simulations. Although promising results showing the potential of both techniques for aneurysm thrombosis prediction have been published recently, there is a lack of cross-validation analysis, which would help in better understanding the limitations of both techniques.

2 Materials and methods

2.1 Preprocessing of medical data

We studied a wide-neck aneurysm of the distal left internal carotid artery from a 58-year-old male, who was treated by FD placement. This aneurysm had a complex morphology with close spatial relationship to the optic nerve, preventing simple coiling to be the first treatment option. In this patient, the initial FD had no effect on the aneurysm size and an occlusion of the aneurysm was only achieved after several treatment sessions including additional coiling and five overlapping FDs implanted. The geometrical data used in this study were obtained by a CT-angiography (reconstructed voxel size: $0.39 \times 0.39 \times 0.75$ mm^3; Sensation 64, SIEMENS) prior to the first FD placement. The segmentation of CT-data was done manually slice-by-slice by an experienced physician using ImageJ64 (imagej.nih.gov). A smoothed STL model of the parent artery with aneurysm was created from the segmented data using the stlwrite-function in MATLAB (MathWorks, Natick, Massachusetts).

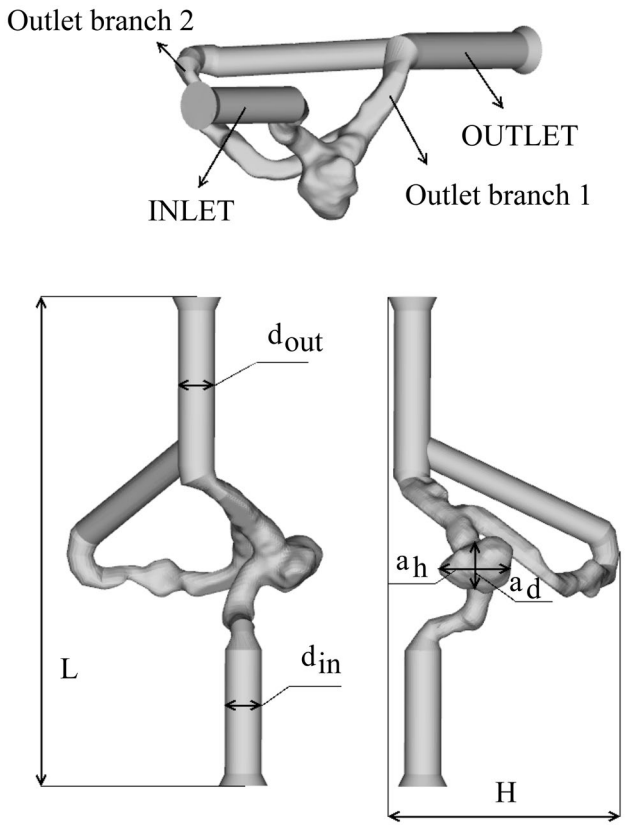

Fig. 1 Geometry of intracranial aneurysm model at different projections: inlet—internal carotid artery; branch 1—middle cerebral artery; branch 2—anterior cerebral artery

Figure 1 shows the geometry of the aneurysm model. Dimensions of the model are presented in Table 1. The aspect ratio (AR) of aneurysm depth to aneurysm neck was 0.86 (Ujiie et al. 2001). According to the study (Brinjikji et al. 2009), such AR requires usage of complicated adjunctive techniques in case of coiling. Therefore, in such a complex case a FD is preferable. To simplify the connection of the model to hoses of the experimental setup, two artificial cylinders were attached to the inlet and outlet branches. Two outlet cylinders were joined to form one outlet segment.

2.2 MRI studies

2.2.1 Experimental model

A patient-specific silicone model was used for experimental studies. The model was created using a lost-wax technique (Sugiu et al. 2003). The obtained STL model of the parent artery with aneurysm was used to print a high precision 3D wax model in a 3D printer. Then the silicone was poured around the wax model. The wax was later removed and thus sustaining a copy of the anatomical structure. Since lost-wax techniques are known to cause susceptibility artifacts/distortions in the MRI data, especially for slow flow measures close to the wall due to wax residue, we conducted a careful visual inspection to ensure that there were no wax residues in the model. The dimensions of the model were the following: length = 76 mm, height = 55 mm and width = 45 mm. The prepared silicone model is presented in Fig. 2. The model was re-imaged with the same CT scanner and protocol to ensure similarity of the created model with the real geometry and estimate an error of fabrication. Differences in geometry were obtained using open-source software CloudCompare (http://www.danielgm.net/cc/), which has been designed to perform direct comparison between dense 3D point clouds. One million sample points were generated for both initial segmentation and reimaged model to obtain point clouds for comparison. Then cloud/cloud distance was computed, providing the following results: average distance = 0.01 mm, max distance = 1.08 mm, sigma = 0.08 mm, max error (distance of the point to the fitted plane) = 0.31 mm, which ensured a good match between the initial segmentation and the fabricated model.

Two copies of the model were used in the study: the first one for preoperative velocity field measurements without FD and the second one for postoperative measurements with the implanted FD. An Acandis DERIVO® Embolisation Device (Acandis GmbH, Pforzheim, Germany) was deployed to the second model copy using the corresponding delivery system. The FD dimensions were the following: diameter was 5.5 mm and length was 20 mm. The position of the FD is shown in Fig. 3a.

Table 1 Dimensions of the parent artery and aneurysm

PA_l	PA_w	d_{in}	d_{iout}	a_h	a_w	a_d	a_n
80	35	5	5	12	11	7	8.13

All dimensions are in mm

PA_l length of parent artery, PA_w width of parent artery, d_{in} and d_{iout} inlet and outlet diameters, a_h aneurysm height, a_w aneurysm width, a_d aneurysm depth, a_n aneurysm neck

Fig. 2 Patient-specific silicone model of the aneurysm of the left internal carotid artery

2.2.2 MR imaging

The MR measurements were performed on a 3 T Philips Ingenia MR Scanner (Philips Healthcare, Best, The Netherlands). The silicone model was placed in a wrist coil for adequate SNR at higher spatial resolutions. Velocity measurements within the aneurysm model were performed by a 4D phase-contrast MR-angiography. The scan protocol comprised scanning with phase encoding in three spatial directions and an additional static measurement without velocity encoding.

Quantitative flow maps were calculated by the Philips scanner software and included magnetic field inhomogeneity correction by the static measurement. For each flow direction, 14 measurements were sampled per cardiac cycle. Image acquisition was performed by a multi-shot 3D turbo field echo (TFE) sequence, a special gradient echo pulse sequence with data acquisition after an initial 180° preparation pulse for contrast enhancement. The acquisition parameters were as follows: TE = 2.9 ms, TR = 6.1 ms, $\alpha = 10°$, TFE factor = 5, acquired voxel size RL × AP × FH = 0.60 × 0.61 × 0.60 mm^3, reconstructed voxel size 0.27 × 0.27 × 0.3 mm^3 and matrix size of 224 × 224 × 187 within a total scan duration of 51 min. The velocity encoding level (VENC) was set to 100 cm/s. The acquired data were manually checked for aliasing in all spatial directions at systolic peak in the aneurysm region.

2.2.3 Experimental setup

Figure 4 shows a scheme of the experimental setup, which was assembled to conduct MRI measurements of blood velocity in the aneurysm model. The following italic numbers are referenced to the scheme as shown in Fig. 4. The MR measurements of the aneurysm model 1 were performed

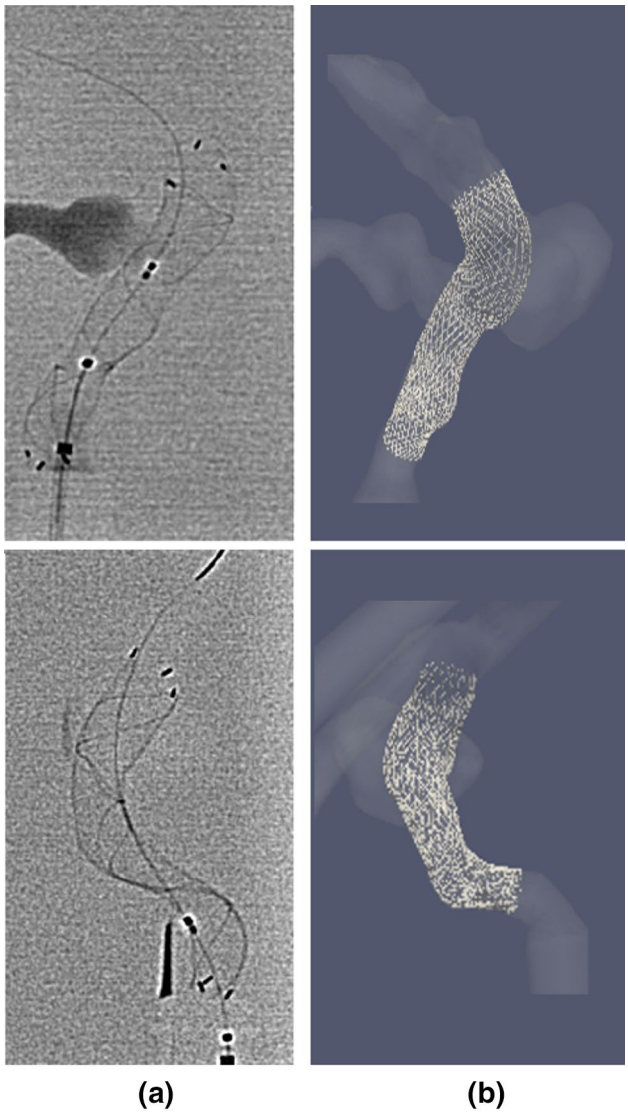

Fig. 3 Flow diverter: **a** angio visualization of flow diverter position: AP projection and LAT projection; **b** flow diverter position after virtual implantation into patient-specific model of cerebral aneurysm

at room temperature. An in-house computer driven piston pump 6, consisting of a linear motor (Linmot, Switzerland) connected to a piston, was used to produce realistic flow conditions. The trigger signal 7 of the piston pump was used as external cardiac gate device for the MR scanner.

The elastic tube 4 and aortic valve 5 (Björk–Shiley) were used to simulate the behavior of the aorta. The inlet flow and outlet pressure were measured using a high-precision flow meter 2 (SWF-4, Zepeda Instruments, Seattle, WA, USA) and pressure transducers 3, 10 (Druck PMP4010, GE Measurement and Control, Billerica, MA, USA), respectively. The pulse frequency of the piston pump was 65 bpm, which combined with the 14 measurements per cycle, results in a temporal resolution of 66 ms. Auxiliary reservoirs 8, 9 were

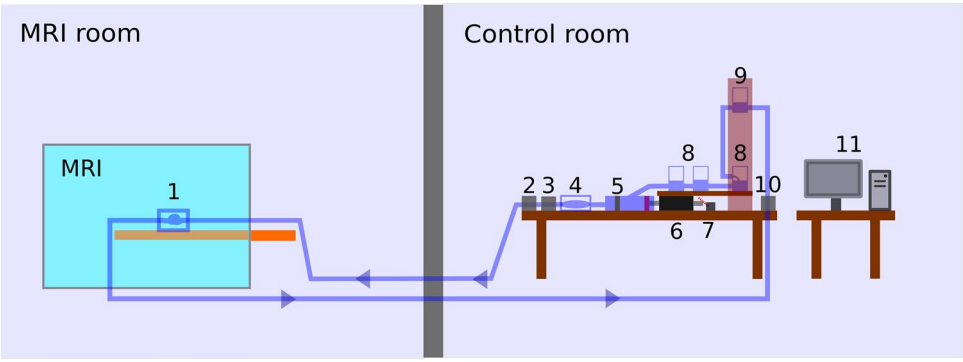

Fig. 4 Scheme of an experimental setup used for MRI measurements of hemodynamic parameters in the patient-specific aneurysm model: 1—silicone model of aneurysm; 2—flow meter; 3—inlet pressure transducer; 4—elastic tube to model the elastic properties of the aorta; 5—aortic valve; 6—piston pump; 7—trigger; 8—lower reservoir; 9—upper reservoir; 10—outlet pressure transducer; 11—computer

used to ensure a constant pressure level. The circulation fluid was a 58% glycerol–water solution, which exhibits Newtonian behavior (Balasso et al. 2014). The fluid had density of 1141 kg/m^3 and the dynamic viscosity of 4.1 mPa·s, which correlate with arterial blood density (1050 kg/m^3) and viscosity (4 mPa s).

2.2.4 Post-processing of MRI data

The MRI data were saved as DICOM files containing magnitude and phase-contrast information for all three directions (FH, AP, RL). The DICOM files were read into MATLAB using the dicomread function. The vessel anatomy was reconstructed by threshold-based semi-automatic segmentation of the magnitude data. This was done slice by slice with correction by an experienced physician. Voxels outside the vessel anatomy were set to have no flow in any direction. No anti-aliasing technique was implemented since the maximum flow in the aneurysm region (85.4 cm/s) was below VENC of 100 cm/s, which was confirmed by careful visual data inspection. For visual representation, the measured velocity data were further post-processed by the Cell Data to Point Data filter in ParaView open-source visualization software (Kitware, USA), which averages the values of the cells surrounding a point to compute a smooth interpolation.

2.3 CFD studies

2.3.1 FD implantation

A geometrical model of the Acandis DERIVO® Embolisation Device was constructed for hemodynamic studies. The FD consisted of 48 Nitinol wires and had the following dimensions according to specifications: the length $S_L = 20$ mm and the diameter $S_D = 5.5$ mm. The wire thickness was 0.04 mm and the braiding angle α was 30°.

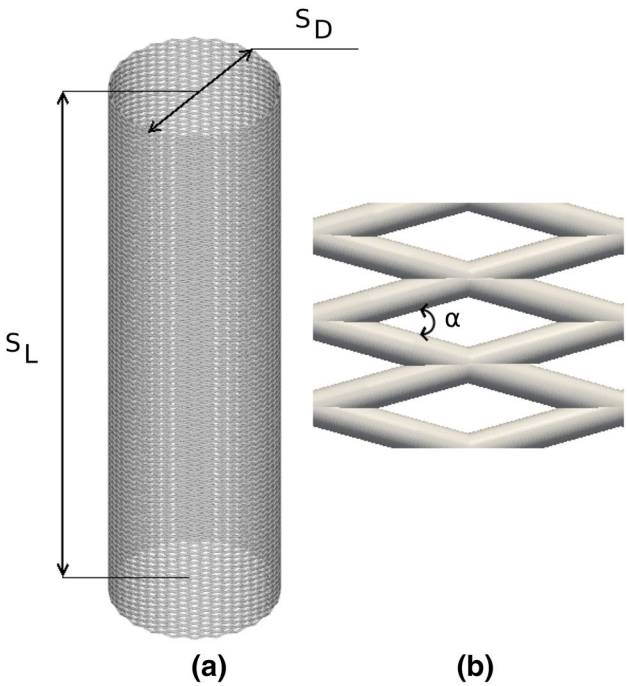

Fig. 5 Geometrical model of flow diverter: **a** isometric projection of the flow diverter model; **b** cells of the flow diverter braid

Figure 5 shows the geometrical model of the FD that was constructed using the open-source 3D modeling software Blender (Blender Foundation, Amsterdam, Netherlands).

The fast virtual stenting technique, proposed by Larrabide et al. (2012) and Bernardini et al. (2012), was used for virtual placement of the FD in the vascular model. The FD struts and their connectivity were defined over a subset of points of a 2-simplex mesh with a size of 4 × 4, which was repeated 24 times circumferentially (resulting in 48 wires, 24 rotating right and 24 rotating left). The position and geometry of the implanted FD are shown in Fig. 3b.

2.3.2 Generation of the computational mesh

To generate a computational mesh for CFD studies, the STL file with the aneurysm geometry was pre-processed: geometrical defects were fixed and aneurysm surface was smoothed to eliminate irregularities caused by segmentation of the medical data.

The snappyHexMesh tool from the OpenFOAM package (CFD Direct, Caversham, England) was used to generate a hexahedral mesh for preoperative and postoperative studies. For preoperative study, a total number of cells were about 6 million. The mesh for postoperative study was generated with higher spatial resolution due to the size of FD wires. The computational mesh consisted of about 20 million cells to ensure the accuracy of blood flow simulation with FD implanted into the aneurysm model. For both cases, a mesh doubling test was conducted to ensure a mesh independence of numerical results.

2.3.3 Simulation of blood flow in cerebral aneurysm

The following assumptions were accepted to simulate the blood flow in the intracranial aneurysm: vessel wall is rigid, blood is incompressible Newtonian fluid, and external forces were neglected.

The governing Navier–Stokes equations were used to describe the flow of blood in the patient-specific model of the cerebral aneurysm:

$$\frac{\partial \vec{u}}{\partial t} = -(\vec{u} \cdot \nabla)\vec{u} + \nu \Delta \vec{u} - \frac{1}{\rho} \nabla P, \tag{1}$$

$$\nu = \frac{\mu}{\rho}, \quad div\ \vec{u} = 0, \tag{2}$$

where $\vec{u}$ is the velocity; ν is the dynamic viscosity; μ is the kinematic viscosity; ρ is the fluid density; P is the pressure.

CFD studies of preoperative and postoperative hemodynamic changes were done using open source software OpenFOAM. The PIMPLE algorithm was used for solving Eqs. (1) and (2). The temporal resolution was 0.0005s. High-performance computing technique was applied to minimize the computational time of the simulation. Therefore, the computational domain was divided into subdomains using Scotch algorithm; each subdomain was processed by a separate computational thread. The "Lomonosov" supercomputer of Moscow State University was used to conduct a HPC-simulation utilizing message passing interface (MPI) technology (Vetter 2015).

2.3.4 Initial and boundary conditions

The flow values measured by the flow meter 2 were used to control performance of piston pump 6 and could not be used as boundary condition for numerical simulations due to relatively large distance between the model and the flow meter and possible damping effect of elastic hoses connecting components of the experimental setup. Therefore, the boundary conditions for CFD simulations were applied according to MRI-measured data. Since the inlet segment of the model is a cylinder, the velocity values for CFD inlet boundary condition were measured at the middle-length of it rather than at the cylinder beginning to minimize measurements errors, which are usually high at the edge of the field of view. Due to relatively large length of connection hoses, we assumed flow entering the model has a developed parabolic profile, which was further checked by 4D Flow MRI measurements. Initially, velocity profile was measured across the inlet segment. Then measured values were post-processed to obtain the average velocity over the cross-section and fully developed Poiseuille profile was generated and imposed at the inlet. The pressure at outlet (mmHg) obtained by experimental studies was converted to kinematic pressure (m^2/s^2) and imposed at outlet. The experimental data were

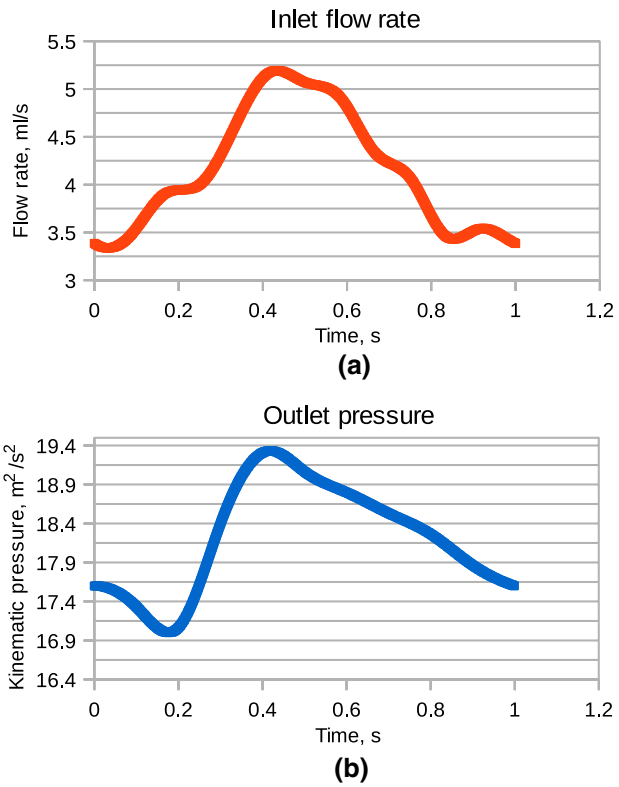

Fig. 6 Boundary conditions for CFD studies: **a** flow rate at the inlet; **b** pressure at the outlet

approximated with cubic splines to eliminate data noise. The curves for inlet flow rate and outlet pressure are shown in Fig. 6. The flow regime was laminar with the Reynolds number at the inlet varied in range from 223 to 333 during the cardiac cycle. Three cardiac cycles were simulated to omit initial perturbations of velocity field in the aneurysm sac and the last, third, cycle was analyzed.

2.4 Flow reduction

The aim of a FD is to redirect a blood flow from the aneurysm sac to its physiological direction along the vessel. To characterize the effect of flow-diversion, a flow reduction R was used. The flow reduction R represents a rate to which an intra-aneurysmal velocity reduces in comparison with preoperative velocity and can be described as:

$$R = \frac{\bar{u}_{\text{pre}} - \bar{u}_{\text{FD}}}{\bar{u}_{\text{pre}}} \times 100\%, \tag{3}$$

where $\bar{u}_{\text{pre}}$ is the average intra-aneurysmal velocity in aneurysm without FD; $\bar{u}_{\text{FD}}$ is the average intra-aneurysmal velocity in aneurysm with implanted FD. We evaluated velocity averaged over space and cardiac cycle for the cases with and without implanted FD. Only the aneurysm volume was considered, excluding the parent artery.

3 Results

3.1 Preoperative analysis

Figure 7a, b shows the velocity distribution at the median plane inside the aneurysm model for CFD and MRI, respectively. Velocity reached its maximum at $t = 0.45$ s, therefore, this moment was used for analysis. Both CFD and MRI results showed a similar flow pattern. The difference for maximum velocity was 9.21%. On both cross-sections the maximum velocity magnitude, 0.684 m/s and 0.621 m/s for CFD and MRI, respectively, was observed at the region near the left side of the aneurysm. The velocity value on the right side of the aneurysm cross-section (in the aneurysm bleb) was about 0.057 m/s for CFD and 0.062 m/s for MRI. The average velocity over cross-section was 0.127 m/s for CFD and 0.132 m/s for MRI. Thus, the difference in average velocity was 3.94%.

The distribution of velocity magnitude for the median cross-section is presented in Fig. 8. A similar distribution pattern was observed for CFD and MRI. For most of the velocity values, the ratios for CFD and MRI results were similar. However, for MRI the low velocity (≤ 0.1 m/s) share was 61%, whereas for CFD it was only 45%.

For a detailed comparison of preoperative hemodynamics, a set of six cross-sections was used. The comparative image of these cross-sections is presented in Fig. 9. A comparative analysis of CFD and MRI data showed that a similar

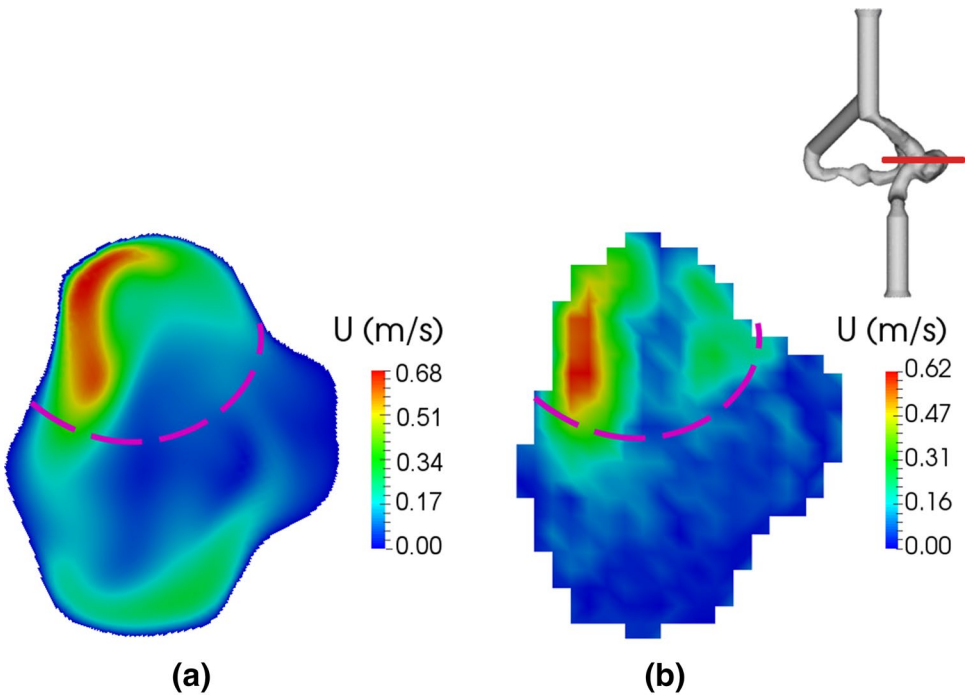

Fig. 7 Velocity magnitude over central cross-section at systolic peak: **a** CFD; **b** MRI. Dashed line corresponds to the neck of the aneurysm

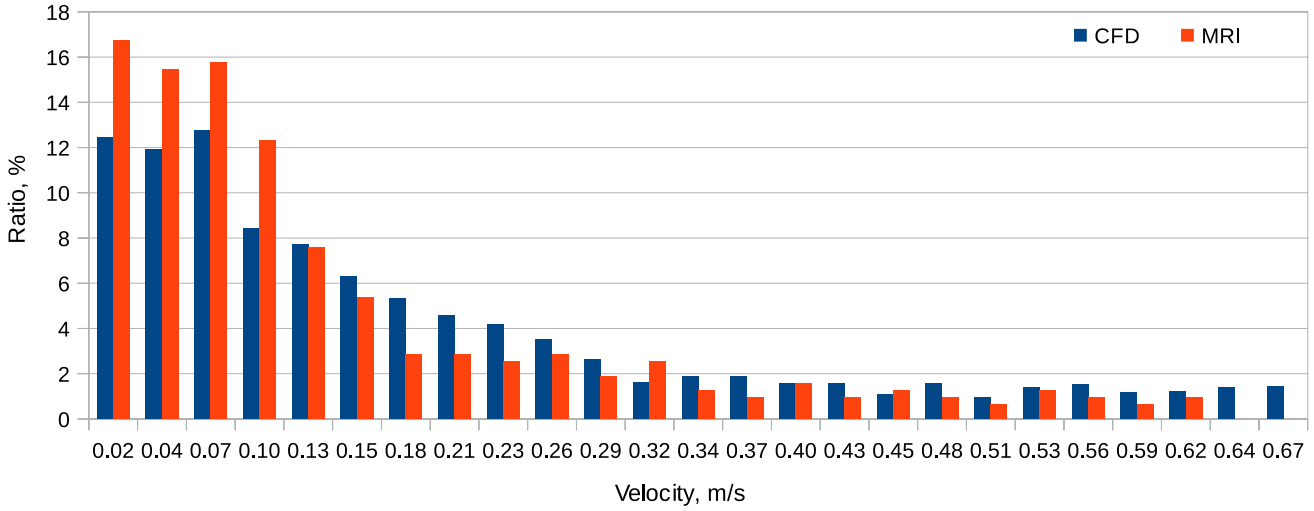

Fig. 8 Distribution of velocity for central cross-section of aneurysm model before stenting at systolic peak

main flow pattern was obtained for each cross-section of the intracranial aneurysm model.

Two control points on the central cross-section were selected to compare a velocity change over the cardiac cycle for CFD and MRI. The first point corresponded to a high velocity zone, which belongs to the parent artery. The second one was located in the center of the aneurysm sac, where the lowest velocity values were observed. A difference between CFD and MRI should be maximal at these points. A position of the control points and obtained velocity curves are presented in Fig. 10. Each MRI value was compared with the corresponding CFD value and an average difference D for each control point was calculated as:

$$D = \frac{1}{N}\sum_{i=1}^{N}\frac{|\mathrm{CFD}_i - \mathrm{MRI}_i|}{\mathrm{CFD}_i} \times 100\%, \tag{4}$$

where N is a number of temporal values for MRI; CFD_i is the ith temporal value for CFD; MRI_i is the ith temporal value for MRI.

The difference between CFD and MRI for the first control point was about 4.75% (for the high velocity zone), while for the second control point it increased to 18.64% (for the low velocity zone).

3.2 Postoperative analysis

Similarly, Fig. 11a, b shows the velocity distribution at the median plane inside the aneurysm model. The FD placement significantly altered the intra-aneurysmal flow pattern. Both CFD and MRI results showed a similar flow pattern postoperative as well as for preoperative case. The maximum velocity values, 1.13 m/s and 0.962 m/s for CFD and MRI, respectively, were observed inside the region enclosed by the FD. For the maximum velocity values, the difference was 14.86%. The metallic FD braid caused a small artifact in the MRI measurements; this region was excluded for analysis of mean velocity over central cross-section. The average velocity over cross-section reduced to 0.112 m/s for CFD and to 0.108 m/s for MRI. Thus, the difference between both methods in average velocity was 3.7% in a case of FD placement.

For the postoperative case, the distribution of velocity magnitude for the median cross-section is presented in Fig. 12. A similar distribution was observed for CFD and MRI results. For MRI results, the ratio of low velocities was 71.1%, whereas for CFD it was only 55%. The comparative image of six cross-sections for CFD and MRI after FD placement is presented in Fig. 13. Again, a similar main flow pattern was observed for CFD and MRI results.

Two control points on the central cross-section were used to compare a velocity change over the cardiac cycle for CFD and MRI after the treatment. A position of the points was similar as for preoperative analysis. For the treated aneurysm, the first control point was located inside the FD. The second control point was in the aneurysm sac near the FD mesh. The position of the control points as well as velocity curves are shown in Fig. 14. Equation (4) was used to calculate a difference between the two methods. The difference for the high velocity zone was 11%, while for the low velocity zone it was 20%. In comparison with the preoperative state, the difference D increased both for high and low velocity zones. It should be caused by the presence of the metallic braid of the FD near the control points, which could potentially affect the results of the MRI measurements.

The obtained MRI and CFD results were averaged over space and cardiac cycle in the aneurysm volume, excluding the parent artery. Equation (3) was used to calculate a flow

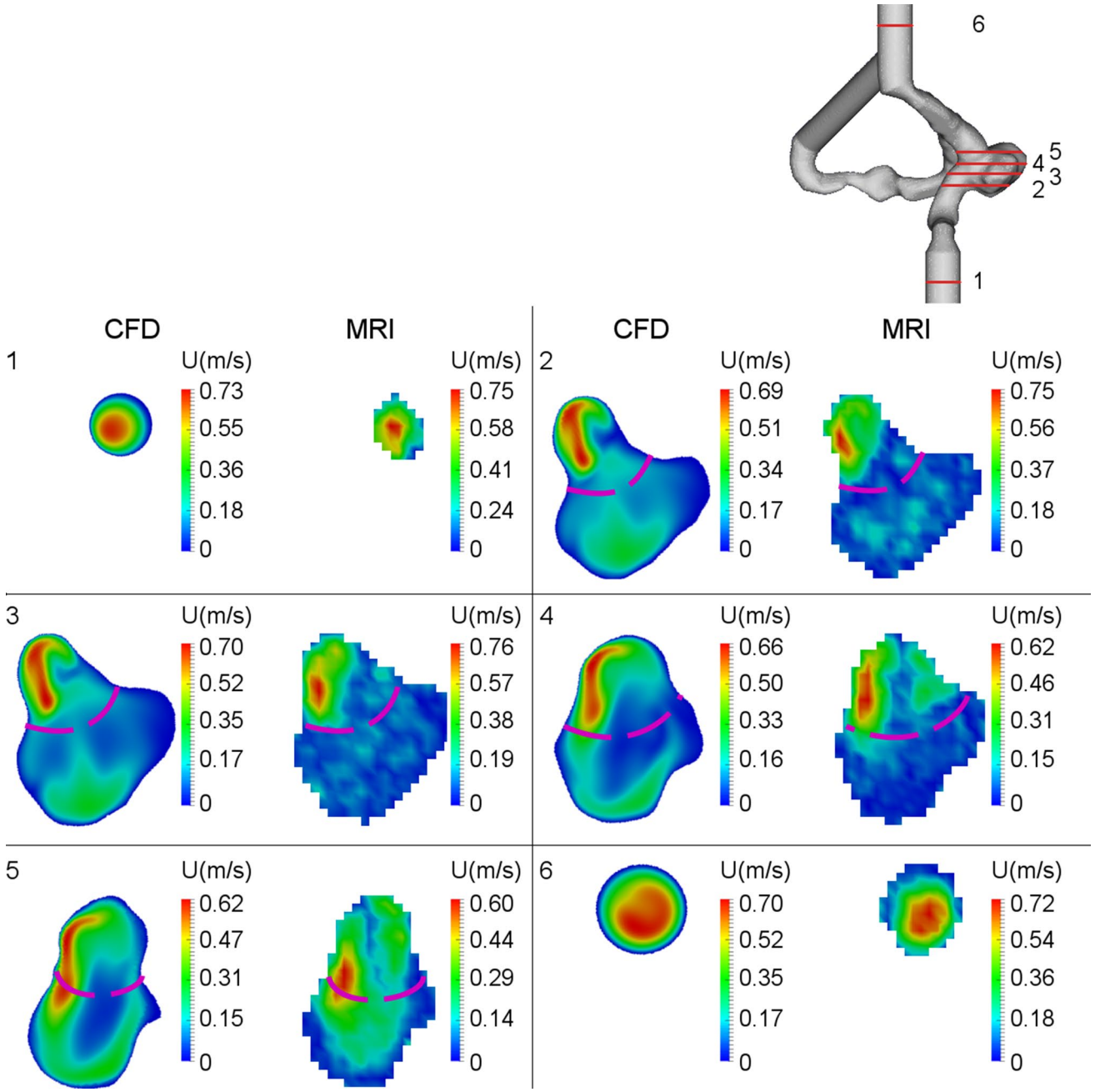

Fig. 9 Velocity map for six different cross-sections of aneurysm model before stenting at systolic peak. From inlet (1) to outlet (6), in each pair: left—CFD; right—MRI

reduction *R* after the FD implantation. For MRI, the flow reduction was 23%, whereas for CFD it was 19%.

4 Discussion

Estimation of intra-aneurysmal flow right after the FD deployment is of great interest for neurointerventionalists and could provide valuable information regarding a flow-diverting effect caused by the implanted stent. One of the clinically applicable methods is 4D flow MRI, which could assess flow reduction in vivo in a significantly less time compared to CFD simulations of the post-treatment flow field (Schnell et al. 2016). Moreover, 4D flow MRI measurements could overcome several limitations of numerical simulations, such as assumption of rigid vessel walls, Newtonian fluid, etc. Several in vivo studies have been done in the recent years evaluating FD performance

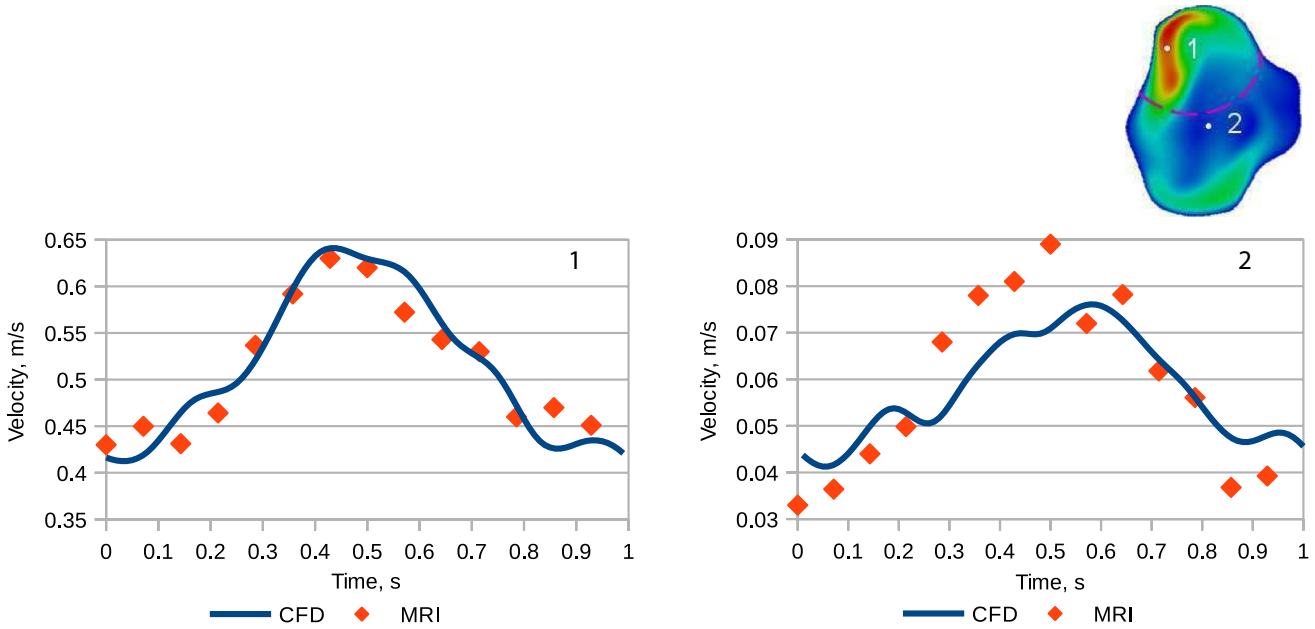

Fig. 10 Velocity over time at the control points before a FD implantation for CFD and MRI

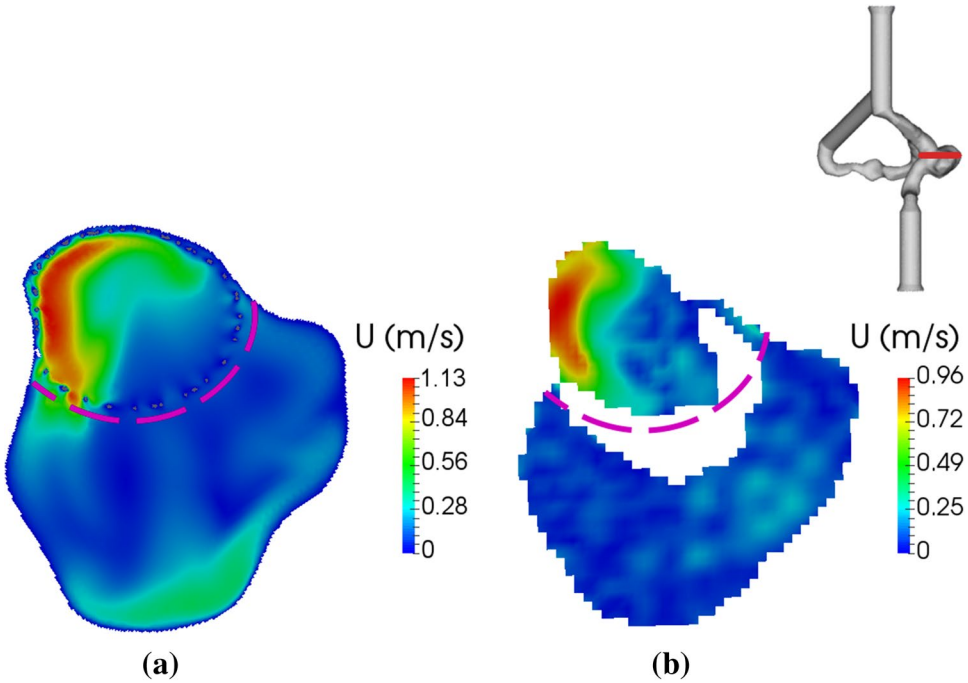

Fig. 11 Velocity map for central cross-section after FD placement at systolic peak: **a** CFD; **b** MRI

after stenting. Thus, MacDonald et al. measured flow alterations in a giant cerebral aneurysm treated with a FD stent both before and after the treatment, and showed that MRI could visualize and assess hemodynamic alterations with sufficient resolution for clinical practice (MacDonald et al. 2015). In another study, intra-aneurysmal flow modifications for ten patients treated with different FDs were assessed by 4D flow MRI as well as problems and limitations of the method were described (Pereira et al. 2015). Nevertheless, in vivo measurements of FD altered flow field are still challenging and more studies required with a large cohort to assess limitations of the method applicability. Moreover, the cross-validation studies between CFD and MRI are necessary to analyze advances and limitations of both methods for evaluation of post-treatment flow changes induced by FD implantation.

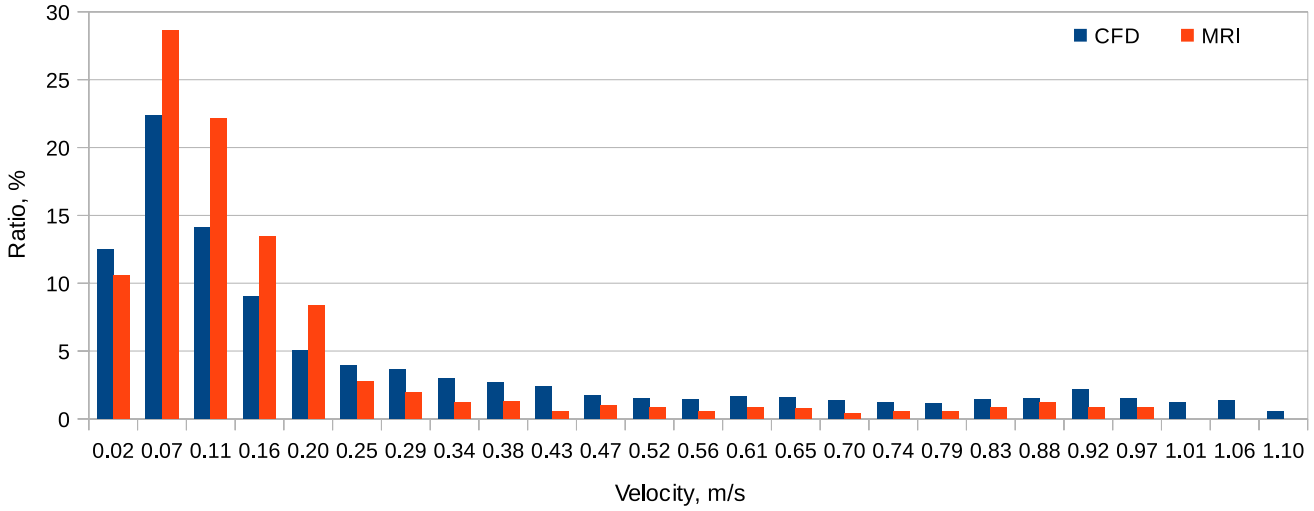

Fig. 12 Distribution of velocity for central cross-section of aneurysm model after FD placement at systolic peak

In the present study, we found a good correspondence between CFD- and MRI-measured velocity both before and after FD treatment. The comparison between CFD and MRI was mostly based on global (averaged) measures of the flow fields. When compared side-by-side, these velocity fields have similar tendencies, but differ more than the averaged values suggest, e.g., the shapes of dominant flow features (e.g., high velocity zones) were frequently in the similar area, but of different shape. Nevertheless, despite low spatial and temporal resolution, the flow pattern in the aneurysm model was correctly measured using 4D flow MRI, which was proven by numerical simulations. As this correspondence persisted after FD placement, we can conclude that our virtual FD placement provided correct boundary conditions for an accurate CFD simulation. Thus, MRI provides a non-invasive way of evaluating the local hemodynamics of cerebral aneurysms after the stent placement. It should be noted that, this is true in our case for an in vitro measurement that took about 50 min of scan time, but not necessarily for a generic 4D flow MRI scan used in vivo due to shorter scan time and additional artifacts. Therefore, further studies required to address this topic.

Matching CFD and experimental MRI data is challenging, as small differences in boundary conditions of CFD and measurement errors in MRI may have large effects on the results. Even temperature changes in the experimental fluid might have an impact on both methods. Boundary conditions were identified with great care and adapted to the MRI scenario; however, in the comparative analysis, we mainly focused on the comparison of flow patterns, main flow features and prioritized a qualitative over a quantitative comparison as displayed in the magnitude flow maps.

Typically, CFD and MRI results require comparison with some in vitro high precision laser-optical methods such as particle image velocimetry (PIV) or laser Doppler anemometer (LDA), which utilize special experimental setup with an aneurysm model as well as experimental blood-like fluid. However, both of these techniques are affected by equipment used and accuracy of an operator. Moreover, the small mismatch in the refractive index between aneurysm wall and fluid may influence the measured velocity field (Ugron et al. 2012). Nevertheless, several studies clearly demonstrated that computed velocity fields agree well with PIV-measured ones if mesh independency is ensured, e.g. (Ford et al. 2008; Raschi et al. 2012). Thus, Cito et al. reported good agreement between CFD and PIV for patient-specific hemodynamics study by six independent research groups during Virtual Intracranial Stenting Challenge 2011 (Cito et al. 2015). The PIV result was reproduced well by each research group and the obtained normalized root-mean-square error was about 7.28%, which is comparable with error in case if different PIV system is used for velocity measurements in the same model (Palero et al. 2010). On the other hand, Frolov et al. compared LDA-measured and CFD-simulated flow fields and found a good agreement between both methods for the patient-specific internal carotid artery aneurysm model (Frolov et al. 2016). Thus, the aforementioned considerations supported our intention to use CFD results as a reference in this study without additional use of LDA or PIV measurements.

Analysis of pre- and post-treatment hemodynamic characteristics showed a flow reduction in the sac of treated aneurysm. There was a good general agreement between MRI-measured and CFD-calculated velocity values (recall Figs. 9, 13). We observed a reduction of blood velocity in both cases: for CFD the reduction of flow in aneurysm sac was 19%, while for MRI data the flow reduction was 23%. However, the obtained flow reduction seems not to

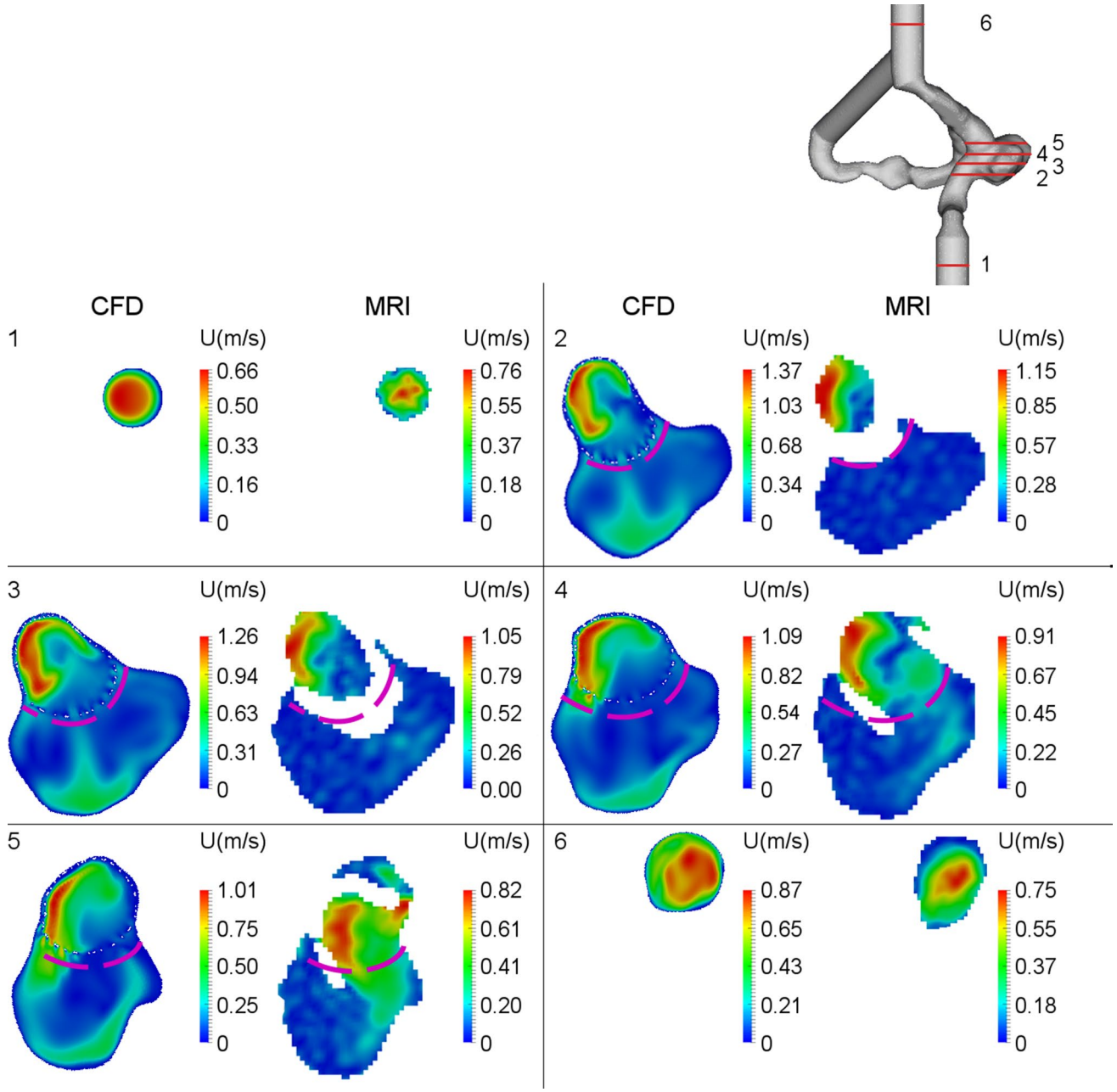

Fig. 13 Velocity map for six different cross-sections of aneurysm model after FD placement at systolic peak. From inlet (1) to outlet (6), in each pair: left—CFD; right—MRI

be sufficient. According to criteria by (Ouared et al. 2016), for successful treatment with FD, the flow reduction should be at least one-third of the initial condition. This statement could potentially explain why the studied aneurysm was unsuccessfully treated with a FD: 6 months after treatment there was still perfusion in the aneurysm dome and occlusion could only be achieved with further treatment.

The individual geometry of a cerebral aneurysm has a significant influence on the distribution of hemodynamic characteristics (Larrabide et al. 2015). The addition of two artificial segments for inlet and outlet could potentially lead to complex flows in the parent artery upstream aneurysm; however, only intra-aneurysmal blood flow was considered in the present study. A Newtonian fluid was used both for MRI measurements and CFD simulations, since the results for Newtonian and non-Newtonian fluids mainly differ only in the low-velocity zones, where the velocities are near zero. However, the spatial resolution of MRI is not high enough to precisely detect these zones, which is demonstrated in our study and agrees well with the recent studies (MacDonald

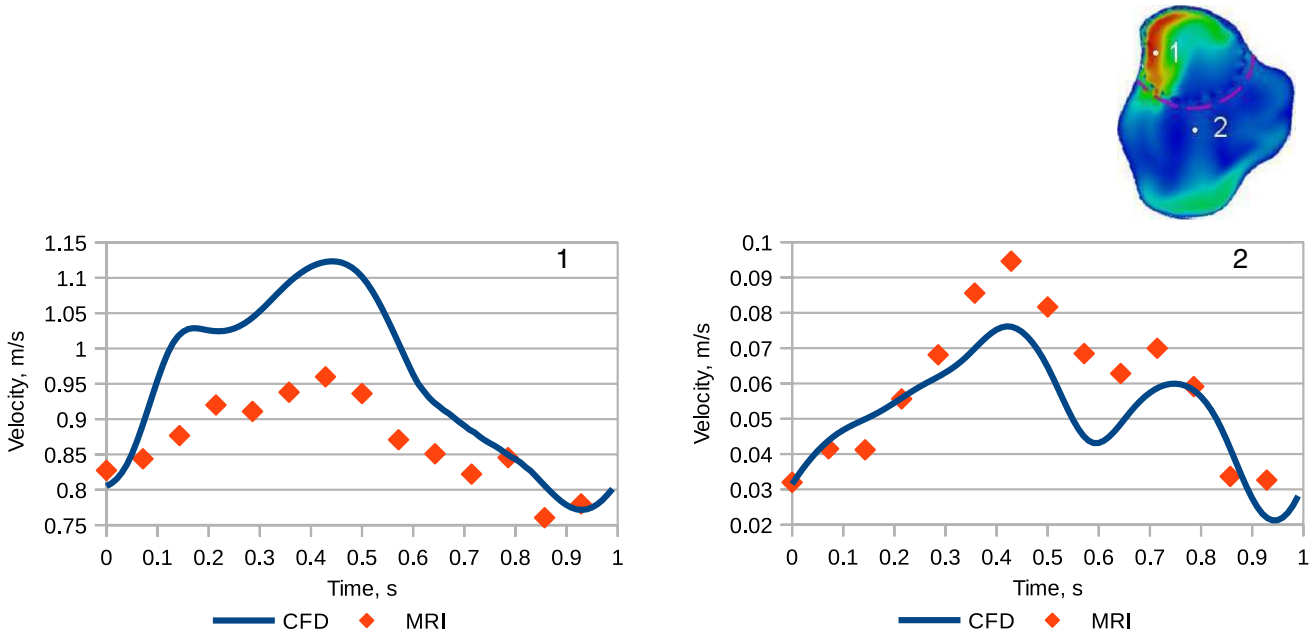

Fig. 14 Velocity over time at the control points after a FD implantation for CFD and MRI

et al. 2015; Pereira et al. 2015). Although a high resolution of the velocity field cannot be achieved by in vivo MRI measurement in intracranial arteries, MRI is able to determine an inlet flow rate with enough precision, which is necessary for a CFD simulation and was used for definition of boundary conditions in the present study. Also the length of the pipes between the piston pump and the phantom in the MR-setup might slightly damp the pulsation. However, the presented data showed clear pulsation to mimic realistic physiological conditions.

The FD geometry and placement also play a significant role on alteration of hemodynamic characteristics in a cerebral aneurysm; however, alterations of cerebral artery shape could be neglected since FD is mechanically soft and cannot expand the lumen substantially. Therefore, only flow alterations caused by stent braiding should be taken into account. In the recent years, there is a trend of utilizing a patient-specific FD placement instead of idealized ones for CFD simulation (Bernardini et al. 2011; Paliwal et al. 2016). Therefore, in the present study, we used a fast virtual stent implantation procedure, provided by Ignacio Larrabide (Bernardini et al. 2012; Larrabide et al. 2012), to obtain a realistic deployment of the FD inside the aneurysm. The comparison between real and virtual deployments showed a good agreement and therefore the deployments could be considered similar. One advantage of MRI compared to CFD is that deployment of FD does not need to be simulated. This omits possible errors which could happen during the virtual deployment of the FD. However, CFD allows simulating different scenarios of FD deployment as well as different types of FDs, which potentially could be used for supporting a physician during a clinical decision making process. Both CFD and MRI methods seem to be complementary; therefore, both of them could be used to use their advantages. On the other hand, MRI is also prone to several measurement errors. In 4D flow MRI, the correct setting for VENC is problematic: it is important to have a good velocity resolution in low flow areas such as in the aneurysm sac, whereas you might encounter aliasing in high velocity regions such as in the FD if the VENC is set too low. To control for these errors, we did not use an aliasing algorithm, but manually inspected the velocity data slice-by-slice. Aliasing was detected only in the in- and outflow vessels, but not in the aneurysm region itself, i.e., in the regions of interest where flow was not altered by aliasing artifacts.

Due to Rician noise in MRI, we expected to overestimate low velocities in the MR measurement which is in compliance with the described higher ratio of velocities < 10 cm/s compared to the CFD simulations, which is in agreement with in vivo studies, e.g., (Pereira et al. 2015). As we compared absolute velocities, the Rician noise is not cancelled out (there are no negative values) and therefore the mean of the noise could introduce a small offset in low flow regions. In addition, possible phase wrapping could contribute to underestimation of high velocities in the studied model, despite it was not observed visually. Limitations of the temporal resolution for the MR measurements might lead to an underestimation of the systolic phase peak. This undersampling artifact contributes to deviations between MRI and CFD flow maps. The increased difference between CFD and

MRI results for the postoperative compared to the preoperative case could be the result of susceptibility artifacts of the metallic FD, which are consisted with previous studies, e.g., (MacDonald et al. 2015; Pereira et al. 2015). The flow diverter caused only a very local signal cancellation in the area of the struts due to weak susceptibility perturbations. The affected voxels were excluded from analysis based on the real images. By comparing the parent vessel just before and inside the flow diverter, no systematic differences were observed in the center of the vessel. Furthermore, the field inhomogeneities, induced by the flow diverter, could cause additional dephasing and thereby phase errors affecting the measured velocities. Careful inspection did not reveal those effects. However, we cannot fully exclude phase errors induced by the flow diverter. To analyze the influence of temporal resolution on flow underestimations might be investigated in further studies.

Partial volume effects might be another error source in MRI (Tang et al. 1993, 1995). However, as the MRI magnitude data showed well defined borders for the vessel anatomy, no artificial resolution enhancement was performed. Slice-by-slice correction by an experienced physician of threshold based semi-automatic segmentation showed very good agreement between anatomy and acquired data. The presented study has some limitations. The study was conducted on a single aneurysm case only, which limits the interpretation of comparison results on aneurysms of different size and shape. Therefore, a number of clinical cases should be extended to evaluate the ability of MRI to precisely estimate the hemodynamic parameters in cerebral aneurysms after FD implantation. The vessel wall was assumed to be rigid. Due to susceptibility artifacts of the metallic FD there is no flow information close to the FD. The algorithm to define the volume of interest should be improved to prevent the exclusion of low-value velocities at the boundaries from measured data. One of the possible ways is to apply a global threshold method proposed in (Otsu 1979). This method can be applied to the histogram of the magnitude data to calculate a global threshold, so the resulting segmentation does not rely on human choices for the boundary. This would be a topic of future studies.

5 Conclusions

In the present study, we investigated hemodynamics in a patient-specific model of a wide-neck aneurysm of the left internal carotid artery. We compared CFD and MRI methods for quantification of intra-aneurysmal flow patterns before and after FD placement. We showed a qualitative and quantitative agreement of velocity fields measured by CFD and MRI both before and after FD placement in a patient-specific model of an intracranial aneurysm. Although the velocity field could not be resolved in high spatial resolution by MRI, MRI was able to correctly determine the main flow pattern in a cerebral aneurysm. While it requires a number of clinical validations, MRI measurements have the potential to be used in future for in vivo evaluation of post-treatment hemodynamic changes induced by FD placement. The pre-treatment CFD simulation could be helpful in predicting the outcome of a FD treatment, which would be of interest for interventional planning.

Acknowledgements We thank Acandis GmbH & Co. KG for providing the DERIVO® Embolisation Device and the silicone model of the aneurysm for the experimental studies. We are grateful to Professor Ignacio Larrabide for conducting a virtual FD implantation into our aneurysm model. The reported study was supported by the Supercomputing Center of Lomonosov Moscow State University.

Funding This work was supported by Russian Science Foundation (Project 16-15-10327).

Compliance with ethical standards

Conflict of interest Dr. J.S. Kirschke received speaker honoraria from Philips Healthcare.

Informed consent As our experiments were conducted retrospectively with permanently anonymized patient data, our local ethics committee deemed the study exempt from the requirement for approval.

References

Balasso A, Bauer JS, Liebig T et al (2014) Evaluation of intra-aneurysmal hemodynamics after flow diverter placement in a patient-specific aneurysm model. Biorheology 51:341–354. https://doi.org/10.3233/BIR-14019

Berg P, Stucht D, Janiga G et al (2014) Cerebral blood flow in a healthy circle of Willis and two intracranial aneurysms: computational fluid dynamics versus four-dimensional phase-contrast magnetic resonance imaging. J Biomech Eng. https://doi.org/10.1115/1.4026108

Bernardini A, Larrabide I, Morales HG et al (2011) Influence of different computational approaches for stent deployment on cerebral aneurysm haemodynamics. Interface Focus 1:338–348. https://doi.org/10.1098/rsfs.2011.0004

Bernardini A, Larrabide I, Petrini L et al (2012) Deployment of self-expandable stents in aneurysmatic cerebral vessels: comparison of different computational approaches for interventional planning. Comput Methods Biomech Biomed Eng 15:303–311. https://doi.org/10.1080/10255842.2010.527838

Boussel L, Rayz V, Martin A et al (2009) Phase-contrast magnetic resonance imaging measurements in intracranial aneurysms in vivo of flow patterns, velocity fields, and wall shear stress: comparison with computational fluid dynamics. Magn Reson Med 61:409–417. https://doi.org/10.1002/mrm.21861

Brinjikji W, Cloft HJ, Kallmes DF (2009) Difficult aneurysms for endovascular treatment: overwide or undertall? AJNR Am J Neuroradiol 30:1513–1517. https://doi.org/10.3174/ajnr.A1633

Cebral JR, Mut F, Raschi M et al (2011) Aneurysm rupture following treatment with flow-diverting stents: computational

hemodynamics analysis of treatment. AJNR Am J Neuroradiol 32:27–33. https://doi.org/10.3174/ajnr.A2398
Chitale R, Zanaty M, Chalouhi N et al (2014) Immediate aneurysm rupture after pipeline embolization: a new complication of flow diversion. Clin Neurol Neurosurg 124:188–191. https://doi.org/10.1016/j.clineuro.2014.07.002
Cito S, Geers AJ, Arroyo MP et al (2015) Accuracy and reproducibility of patient-specific hemodynamic models of stented intracranial aneurysms: report on the Virtual Intracranial Stenting Challenge 2011. Ann Biomed Eng 43:154–167. https://doi.org/10.1007/s10439-014-1082-9
Darsaut TE, Rayner-Hartley E, Makoyeva A et al (2013) Aneurysm rupture after endovascular flow diversion: the possible role of persistent flows through the transition zone associated with device deformation. Interv Neuroradiol J Perither Neuroradiol Surg Proc Relat Neurosci 19:180–185. https://doi.org/10.1177/159101991301900206
Ford MD, Nikolov HN, Milner JS et al (2008) PIV-measured versus CFD-predicted flow dynamics in anatomically realistic cerebral aneurysm models. J Biomech Eng 130:021015. https://doi.org/10.1115/1.2900724
Frolov SV, Sindeev SV, Liepsch D, Balasso A (2016) Experimental and CFD flow studies in an intracranial aneurysm model with Newtonian and non-Newtonian fluids. Technol Health Care Off J Eur Soc Eng Med 24:317–333. https://doi.org/10.3233/THC-161132
Isoda H, Hirano M, Takeda H et al (2006) Visualization of hemodynamics in a silicon aneurysm model using time-resolved, 3D, phase-contrast MRI. AJNR Am J Neuroradiol 27:1119–1122
Karmonik C, Zhang YJ, Diaz O et al (2014) Magnetic resonance imaging as a tool to assess reliability in simulating hemodynamics in cerebral aneurysms with a dedicated computational fluid dynamics prototype: preliminary results. Cardiovasc Diagn Ther 4:207–212. https://doi.org/10.3978/j.issn.2223-3652.2014.02.07
Kono K, Terada T (2014) Flow visualization of recurrent aneurysms after coil embolization by 3D phase-contrast MRI. Acta Neurochir (Wien) 156:2035–2040. https://doi.org/10.1007/s00701-014-2231-5
Kulcsár Z, Houdart E, Bonafé A et al (2011) Intra-aneurysmal thrombosis as a possible cause of delayed aneurysm rupture after flow-diversion treatment. AJNR Am J Neuroradiol 32:20–25. https://doi.org/10.3174/ajnr.A2370
Larrabide I, Kim M, Augsburger L et al (2012) Fast virtual deployment of self-expandable stents: method and in vitro evaluation for intracranial aneurysmal stenting. Med Image Anal 16:721–730. https://doi.org/10.1016/j.media.2010.04.009
Larrabide I, Geers AJ, Morales HG et al (2015) Effect of aneurysm and ICA morphology on hemodynamics before and after flow diverter treatment. J NeuroInterv Surg 7:272. https://doi.org/10.1136/neurintsurg-2014-011171
MacDonald ME, Dolati P, Mitha AP et al (2015) Hemodynamic alterations measured with phase-contrast MRI in a giant cerebral aneurysm treated with a flow-diverting stent. Radiol Case Rep 10:1109. https://doi.org/10.2484/rcr.v10i2.1109
Muir ER, Watts LT, Tiwari YV et al (2014) Quantitative cerebral blood flow measurements using MRI. Methods Mol Biol Clifton NJ 1135:205–211. https://doi.org/10.1007/978-1-4939-0320-7_17
Mut F, Raschi M, Scrivano E et al (2015) Association between hemodynamic conditions and occlusion times after flow diversion in cerebral aneurysms. J Neurointerv Surg 7:286–290. https://doi.org/10.1136/neurintsurg-2013-011080
Naito T, Miyachi S, Matsubara N et al (2012) Magnetic resonance fluid dynamics for intracranial aneurysms—comparison with computed fluid dynamics. Acta Neurochir (Wien) 154:993–1001. https://doi.org/10.1007/s00701-012-1305-5
Otsu N (1979) A threshold selection method from gray-level histograms. IEEE Trans Syst Man Cybern 9:62–66. https://doi.org/10.1109/TSMC.1979.4310076
Ouared R, Larrabide I, Brina O et al (2016) Computational fluid dynamics analysis of flow reduction induced by flow-diverting stents in intracranial aneurysms: a patient-unspecific hemodynamics change perspective. J Neurointerv Surg. https://doi.org/10.1136/neurintsurg-2015-012154
Palero VR, Lobera J, Arroyo MP (2010) Three-component velocity field measurement in confined liquid flows with high-speed digital image plane holography. Exp Fluids 49:471–483. https://doi.org/10.1007/s00348-009-0813-4
Paliwal N, Yu H, Xu J et al (2016) Virtual stenting workflow with vessel-specific initialization and adaptive expansion for neurovascular stents and flow diverters. Comput Methods Biomech Biomed Eng 19:1423–1431. https://doi.org/10.1080/10255842.2016.1149573
Papaharilaou Y, Doorly DJ, Sherwin SJ (2001) Assessing the accuracy of two-dimensional phase-contrast MRI measurements of complex unsteady flows. J Magn Reson Imaging JMRI 14:714–723
Papathanasopoulou P, Zhao S, Köhler U et al (2003) MRI measurement of time-resolved wall shear stress vectors in a carotid bifurcation model, and comparison with CFD predictions. J Magn Reson Imaging JMRI 17:153–162. https://doi.org/10.1002/jmri.10243
Pereira VM, Brina O, Delattre BMA et al (2015) Assessment of intra-aneurysmal flow modification after flow diverter stent placement with four-dimensional flow MRI: a feasibility study. J Neurointerv Surg 7:913–919. https://doi.org/10.1136/neurintsurg-2014-011348
Pierot L, Wakhloo AK (2013) Endovascular treatment of intracranial aneurysms: current status. Stroke 44:2046–2054. https://doi.org/10.1161/STROKEAHA.113.000733
Raschi M, Mut F, Byrne G et al (2012) CFD and PIV analysis of hemodynamics in a growing intracranial aneurysm. Int J Numer Methods Biomed Eng 28:214–228. https://doi.org/10.1002/cnm.1459
Rouchaud A, Brinjikji W, Lanzino G et al (2016) Delayed hemorrhagic complications after flow diversion for intracranial aneurysms: a literature overview. Neuroradiology 58:171–177. https://doi.org/10.1007/s00234-015-1615-4
Schnell S, Wu C, Ansari SA (2016) Four-dimensional MRI flow examinations in cerebral and extracerebral vessels—ready for clinical routine? Curr Opin Neurol 29:419–428. https://doi.org/10.1097/WCO.0000000000000341
Sugiu K, Martin J-B, Jean B et al (2003) Artificial cerebral aneurysm model for medical testing, training, and research. Neurol Med Chir (Tokyo) 43:69–72 **(discussion 73)**
Tang C, Blatter DD, Parker DL (1993) Accuracy of phase-contrast flow measurements in the presence of partial-volume effects. J Magn Reson Imaging JMRI 3:377–385
Tang C, Blatter DD, Parker DL (1995) Correction of partial-volume effects in phase-contrast flow measurements. J Magn Reson Imaging JMRI 5:175–180
Turowski B, Macht S, Kulcsár Z et al (2011) Early fatal hemorrhage after endovascular cerebral aneurysm treatment with a flow diverter (SILK-Stent): do we need to rethink our concepts? Neuroradiology 53:37–41. https://doi.org/10.1007/s00234-010-0676-7
Ugron Á, Farinas M-I, Kiss L, Paál G (2012) Unsteady velocity measurements in a realistic intracranial aneurysm model. Exp Fluids 52:37–52. https://doi.org/10.1007/s00348-011-1206-z
Ujiie H, Tamano Y, Sasaki K, Hori T (2001) Is the aspect ratio a reliable index for predicting the rupture of a saccular aneurysm? Neurosurgery 48:495–502 **(discussion 502–503)**
van Ooij P, Schneiders JJ, Marquering HA et al (2013) 3D cine phase-contrast MRI at 3 T in intracranial aneurysms compared with patient-specific computational fluid dynamics. AJNR Am J Neuroradiol 34:1785–1791. https://doi.org/10.3174/ajnr.A3484

Vetter JS (ed) (2015) Contemporary high performance computing: from petascale toward exascale. CRC Press, Taylor & Francis Group, CRC Press is an imprint of the Taylor & Francis Group, an informa business, Boca Raton

Walcott BP, Stapleton CJ, Choudhri O, Patel AB (2016) Flow diversion for the treatment of intracranial aneurysms. JAMA Neurol 73:1002–1008. https://doi.org/10.1001/jamaneurol.2016.0609

Wong GKC, Kwan MCL, Ng RYT et al (2011) Flow diverters for treatment of intracranial aneurysms: current status and ongoing clinical trials. J Clin Neurosci Off J Neurosurg Soc Australas 18:737–740. https://doi.org/10.1016/j.jocn.2010.10.011

Zanaty M, Chalouhi N, Tjoumakaris SI et al (2014) Flow-diversion panacea or poison? Front Neurol 5:21. https://doi.org/10.3389/fneur.2014.00021